IMPINGEMENT HEAT TRANSFER: CHT CFD PREDICTIONS OF THE INFLUENCE OF REDUCED CROSSFLOW USING LARGE GAPS

Abubakar M. El-Jummah[1], Reyad A. A. Abdul Hussain[2], *Gordon E. Andrews[2] and John E. J. Staggs[2]
[1]Department of Mechanical Engineering, Faculty of Engineering, University of Maiduguri, Nigeria
[2]Energy Research Institute, School of Chemical and Process Engineering, University of Leeds, UK*

*E-mail: profgeandrews@hotmail.com

ABSTRACT

Experimental and Numerical investigations were carried out on impingement jet cooling, for variable gap to diameter ratio Z/D ranging from 0.76 - 6.42 with varied Z, constant D and constant mass flux G of 1.93 kg/sm^{2}bar, which is typical of G for regenerative backside cooling of gas turbine combustors. This is the cooling geometry relevant to reverse flow cylindrical combustors with low NOx burner where air used for film cooling increases the NOx. The geometries investigated were for 10×10 square array of impingement jet cooling holes at constant diameter D and pitch X, hence constant X/D ratio. The experimental results used the lumped capacity method to determine the locally surface average heat transfer with thermocouples spaced at 25.4 mm intervals in the direction of the single exit flow 152.4 mm long impingement gap. The target walls were 6.35 mm thick Nimonic-75 alloy materials that were electrically heated to about 353 K with a coolant air temperature of 288 K. Conjugate heat transfer (CHT) computational fluid dynamics (CFD) were applied to the same geometries. The predicted CFD results agreed with the measured pressure loss, which indicates that the predicted aerodynamics were good. Also, the locally X^2 and overall surface average heat transfer coefficients (HTC) h were well predicted, apart from at the lowest Z/D. The pressure loss increased significantly for Z/D <3 and h also increased but this was not a practical design due to the excessive pressure loss.

NOMENCLATURE

A	[-]	Impingement hole porosity = $[(\pi/4)D^2]/X^2$
D	[m]	Impingement air hole diameter
C_d	[-]	Discharge coefficient
G	[kg/sm^{2}bar]	Coolant mass flux
h	[W/m^{2}K]	Heat transfer coefficient (HTC)
I	[-]	Cross-flow interference parameter
k	[W/mK]	Thermal Conductivity
L	[m]	Test plates metal wall thickness
m'	[kg/s]	Coolant mass flow rate per hole
n	[m^{-2}]	Number of impingement hole/unit surface area
N	[-]	Number of upstream rows of impingement holes
Nu	[-]	Nusselt Number (hD/k_f)
ΔP	[Pa]	Impingement wall pressure loss
P	[Pa]	Coolant supply static pressure (approx. 1bar)
q''	[W/m^2]	Heat flux
R	[J/kgK]	Gas constant for air (287)
Re	[-]	Impingement hole Reynolds number (V_jD/ν)
T	[K]	Temperature
T*	[-]	Dimensionless temperature, Eq.7
U	[m/s]	Impingement gap cross-flow velocity at hole N
V	[m/s]	Impingement jet mean velocity
w	[m]	Target wall total cooled length
X	[m]	Impingement hole square array pitch
y	[-]	Dimensionless pressure loss ratio
Z	[m]	Impingement gap

Special Characters

ρ	[kg/m^3]	Density of air
ν	[m^2/s]	Kinematic viscosity
y$^+$	[-]	Inner variable wall normal coordinate ($\xi U\tau/\nu$)
γ	[-]	Reynolds number exponent
ξ	[m]	Grid cell size
μ	[kg/ms]	Dynamic viscosity
τ	[kg/ms^2]	Wall shear stress,

Subscripts

c	Cross-flow	h	Hole
L	Local	o	Outlet
j	Jet	s	Surface
w	Wall	∞	Coolant

INTRODUCTION

Gas turbine (GT) combustor and turbine blade and nozzle metal walls operate in hot gas flow temperatures well above the metal melting point. The metal surface temperature is kept below the point of loss of strength by a combination of ceramic insulation, internal air cooling systems and external film cooling. Impingement cooling is one of the most common systems of internal air cooling [1] and has complex aerodynamics when used in the absence of associated film or effusion cooling, which are the subject of this conjugate heat transfer (CHT) computational fluid dynamics (CFD) investigation.

Cooling the combustor using wall backside regenerative impingement cooling is necessary in ultra-low NOx gas turbine combustors, as any air for film cooling is air not available for the low NOx primary zone which means that the primary zone operates hotter with higher NOx emissions [2]. Regenerative cooling of low NOx combustors has been adopted in industrial gas turbines [3] as part of ultra-low NOx combustor designs. Regenerative combustor cooling is the main application of the present work and the geometry and coolant flow rate studied are for this application.

Increasing the thermal efficiency of gas turbines with higher operating temperatures is reliant on more effective cooling of metal

1

surfaces. The use of impingement air jet cooling technologies in GTs has been characterized by high heat transfer rates with better cooling effectiveness [4-6]. A feature of impingement cooling is the outflow from the impingement gap, as shown in Fig.1, which increases in velocity with distance along the gap. The ratio of the impingement gap Z, to impingement air hole diameter D (Z/D) is a key impingement heat transfer parameter, as it controls the jet velocity at the impingement wall as well as the crossflow velocity. As the gap size changes, both the jet velocity U_j on the impingement wall and the velocity of the cross flow U_c in the gap will change. However, experimental evidence shows that impingement heat transfer is relatively weak function of Z/D for Z/D < ~4 [1, 3-17].

One feature of impingement heat transfer that is difficult to understand is the influence of crossflow, shown schematically in Fig. 1. Although maximum heat transfer at the impingement points is observed, the additional effect of crossflow would be expected to increase the heat transfer over the entire plate surface. This is not the case in practice, as with high X/D or high impingement jet velocities the heat transfer deteriorates with axial distance [1, 5-11]. The crossflow velocity is inversely proportional to Z/D and so the adverse effect of crossflow on impingement heat transfer ought to be small when Z/D is high. However, this is not the case experimentally [9-11] and the present work was undertaken to better understand the influence of crossflow on impingement heat transfer. This crossflow effect limits the application of impingement cooling in gas turbine combustor wall cooling [3, 18], where longer cooling distances are used compared with turbine blades.

Several experimental investigations have shown that Z/D has little or no effect on the target wall heat transfer at low Z/D and there is a critical Z/D beyond which increases in Z/D lead to a reduction in heat transfer [10-11]. Andrews and Hussain [5] showed that flow maldistribution (an unequal distribution of coolant air mass flow in the jet holes, due to the pressure gradient in the impingement gap) becomes very important for the conditions where impingement jet deflections are likely to be significant. Varying the impingement gap also contributes to the influence of flow maldistribution as a result of the crossflow effect controlling the pressure loss along the impingement cooled duct.
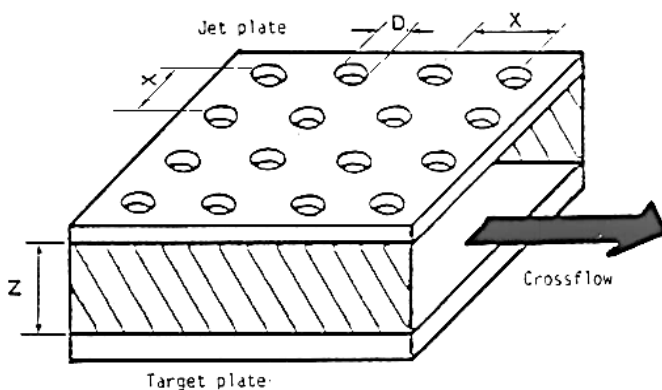

Fig.1: Multijet Impingement cooling geometry showing the coolant outlet direction crossflow [5]

REVIEW OF LITERATURE
Impingement Gap to Diameter Ratio Z/D

Freidman and Mueller [10] found that the impingement heat transfer coefficient, *h,* depended on Z/D. Decreasing the jet diameter D at the same Z/D results in an increase in X/D and higher impingement jet velocities for the same G. For this same Z/D there is a smaller impingement gap Z and higher crossflow velocities [7] which gives more interaction with the impingement jets and greater reduction in heat transfer with axial distance. This shows that Z/D is not the most important impingement cooling design parameter. Huang [11] showed that for small Z/D, the *h* did not show any significant changes. Hollworth and Berry [12] showed that impingement heat transfer had little change in *h for* Z/D<5. Haung [11] found an increase in *h* for increased Z/D without crossflow at constant jet Reynolds number. Saad et al. [13] found that *h* increased with Z/D, which is contrary to most other investigators.

Andrews et al. [15] reviewed the influence of Z/D on *h* for 1 < Z/D < 10 [15] and 1 < Z/D < 6 [1], they concluded that for an X/D of 11 Z/D had little influence on *h* up to a Z/D of 6. For higher Z/D *h* decreased slowly with increase in Z/D. The Z/D effect at variable Z and constant D was dominated by the influence of X/D. A greater effect on *h* was found for constant Z with variable D, which was primarily because this was achieved at constant X and hence the impingement X/D was decreased as D increased, which reduced the impingement jet velocity for the same G [17]. The impingement jet deflection was small as a result of the crossflow effect at large Z/D. With a smaller Z/D of 1.6 at constant X/D, crossflow was not a major factor due to the higher jet velocities [5].

Abdul Husain and Andrews [5] investigated the axial variation of the impingement heat transfer coefficient on the centreline between the impingement holes using a hot metal wall test rig. The results showed that for Z/D > 2, *h* decreased downstream of the impingement cooled wall due to the influence of the crossflow. For small Z/D the crossflow was greatest and this created the highest pressure loss along the impingement gap. This pressure loss can then create a flow maldistribution between the impingement holes. This is also influenced by the X/D as this controls the impingement jet velocity and impingement wall pressure loss. An X/D of 5 was found to be the smallest X/D at which flow maldistribution was small at practical Z/D values. This was the geometry studied in the present work and Z/D was varied so that flow maldistribution occurred at low Z/D < 2 and was not significant at Z/D > 4 [5]

The effect of flow maldistribution is to increase the heat transfer at the trailing edge of the impingement gap, whereas with no flow maldistribution the heat transfer decreased with axial distance along the gap. The experimentally observed trends for Z/D were investigated using conjugate heat transfer CFD, in order to understand better the complex influence of Z/D. The other objective of the work was to show that conjugate heat transfer CFD could predict metal temperatures and heat transfer coefficients in hot wall experiments and hence be reliably applied to engine predictions.

2

Effects of Crossflow

Jets impinging on the opposite target wall are deflected by the crossflow, which reduces h. Metzger and Korstad [15] reported that square arrays of circular jets impinging on a plane surface, which are constrained to exhaust on one side of the array only, as shown in Fig.1, results in a crossflow in the gap which increases in magnitude with distance along the gap. This crossflow interacts with the impingement jets with two effects dependent on the X/D and Z/D [1, 5, 8, 15, 17]. At low X/D, which gives a low impingement wall pressure loss, there is a flow maldistribution set up between the first and last holes in the impingement gap [12] and this results in h increasing with distance along the gap [17]. At high X/D, which gives high impingement jet pressure loss and high jet velocities, there is little flow maldistribution but the heat transfer is deteriorated by the crossflow in the downstream direction [8]. The present work investigates impingement heat transfer at X/D = 4.7 where the two effects of crossflow can be generated by varying the Z/D.

Chance [8] showed that the geometrical influence of the crossflow in the absence of flow maldistribution could be correlated by the parameter I_c, defined by Eq.1, which Andrews and Husain [5] showed was related to the design parameters of impingement cooling X/D, Z/D and to the number of upstream rows of holes, N. The decline in h with axial distance along Z was correlated for X/D >4 (no flow maldistribution) by Chance [8] and converted by Andrews and Hussain [5] into Eq. (2).

$$I_c = \frac{G_c Z}{G_j D} = \frac{\rho_c u_c Z}{\rho_j u_j D} \approx \frac{u_c Z}{u_j D} = \frac{NAX}{D} = \frac{\pi ND}{4X} \quad (1)$$

$$Nu/Nu_o = 1 - 0.185\, ND/X \quad (2)$$

Eq. 2 shows that the deterioration of h with axial distance is a linear function of the number of upstream rows of impingement jets, N, and inversely proportional to X/D.

Review of impingement Cooling CFD Investigations

The complex recirculation in the impingement gap and the interaction between adjacent jets on the target surface presents a challenge for CFD predictions of multi-row impingement cooling with single sided exit. Jet impingement with crossflow for a flat target wall with single sided exit was predicted by Bailey *et al*. [19] for a small number of impingement holes. Previous CFD investigations directed at the cross flow effect have not used a large number of upstream holes. The distribution of heat transfer coefficient h, on the target surface have been well predicted in agreement with liquid crystal based experimental measurements [19, 20]. Both unstructured [21] and hybrid [22] grids have been used depending on the geometry.

Andrews *et al*. [23] computed the internal aerodynamics and turbulence interactions and surface averaged h with a relatively coarse grid and k-e turbulence model. Only CFD was used,

with no internal wall conduction effects. A 100 kW heat flux was modelled and the surface averaged heat transfer coefficients were predicted. This work showed the complexity of the aerodynamics in the impingement gap and had reasonable agreement with surface averaged experimental results for h. This showed that the influence of crossflow was the convection of surface turbulence downstream of the impingement point and the generation of flow and turbulence on the impingement jet surface. El-Jummah *et al*. [24] used CFD/CHT to predict the same geometry using structured grids with a much finer grid and with CHT. The aerodynamics were similar to those with the coarser grid. The CHT enabled the thermal gradients in the wall to be predicted and the overall cooling effectiveness.

The authors have used CHT/CFD to predict various configurations of impingement cooling for a constant Z of 10mm, for which a range of experimental results for hot metal wall rigs are available [7, 14, 25, 26] and further experimental results are presented in the present work. The experimental results for the surface averaged heat transfer coefficient, h, used the transient cooling method of Abdul Hussain *et al*. [7, 14]. The present CFD procedures have been used previously [24, 27-31] to predict the experimental results of Abdul Hussain et al. [7, 14] with good agreement with the experimental h. This work was mainly for a constant Z. The influence of Z/D has been predicted previously based on 100kW heat flux and the wall temperature distribution was predicted [24]. In the present work the conditions of the experimental measurements of h were modelled rather than the hot wall cooling effectiveness as in the previous work [24].

IMPINGEMENT COOLING GEOMETRIES MODELLED

This work was undertaken to understand in more detail the aerodynamic and heat transfer interactions of varying Z/D with a constant D of 3.27mm. The geometries investigated are summarised in Table 1 and were a square array of 10×10 impingement jet cooling holes with Z/D varied from 0.76 - 6.42 at constant X/D of 4.7. The wall thickness was 6.35mm.

Table 1 Geometries for n of 4306 m^{-2} and X/D of 4.7

Z/D	6.42	4.89	3.67	3.06	2.14	1.22	0.76
Z mm	21.0	16.0	12.0	10.0	7.0	4.0	2.5
D mm	3.27	3.27	3.27	3.27	3.27	3.27	3.27
X mm	15.2	15.2	15.2	15.2	15.2	15.2	15.2
n m^{-2}	4306	4306	4306	4306	4306	4306	4306

A fixed coolant mass flux G of 1.93 kg/sm^2 was used as this corresponds to combustor wall cooling using regenerative cooling. All the combustor air flow is used first to cool the wall before entering a low NOx combustion chamber and for typical combustor geometries that gives a G of about 2 kg/sm^{2}bar. The pressure loss at this flow rate at high Z/D was 2.0% and this is at the upper end of the allowable pressure loss, if there is to be sufficient pressure loss left for the low NOx combustor. The impingement hole flow velocity, V_j, and the crossflow velocity at the duct exit, V_c, are given in Table 2. The impingement hole Re was 9,100. Andrews and Hussain (1) have previously investigated the influence of Z/D

3

Table 2 Flow Conditions for a Fixed G of 1.93 kg/sm²bar

Z/D	6.42	4.89	3.67	3.06	2.14	1.22	0.76
V_j (m/s)	43.4	43.4	43.4	43.4	43.4	43.4	43.4
V_c (m/s)	95.7	59.8	34.2	23.9	19.9	15.0	11.4
V_j/V_c	0.5	0.7	1.3	1.8	2.2	2.9	3.8

for an impingement jet wall with X/D of 11 and higher jet Re, using the same equipment as in the present work shown in Fig. 2, but with a steady state method for measuring h.

The coolant mass flow is related to the flow pressure loss across the impingement holes by the basic orifice plate mass flow equation, as in Eq. 3.

$$m' = C_d A_h (2\rho\Delta P)^{0.5} \qquad (3)$$

where m' is the coolant mass flow, kg/s
  A_h is the hole flow area, m²
  C_d is the hole discharge coefficient
  ρ is the upstream air density
  ΔP is the static pressure loss across the hole

Eq. 3 can be rearranged into Eq. (4)

$$G = 10^5 C_d A [(2/RT)(\Delta P/P)]^{0.5} \quad \text{kg/sm}^2\text{bar} \qquad (4)$$

where A = porosity = $\pi / [4(X/D)^2]$
  R = gas constant for air, 287.04 J/kgK
  T = coolant air temperature, K
  $\Delta P/P$ = pressure loss as a % of the upstream absolute
      pressure

Eq. 4 enables the flow conditions at atmospheric pressure to be related to those at any pressure.

The expression in Eq. 4 of the coolant mass flow G per surface area of the wall is proportional to the mean velocity over the entire surface area to be cooled. Eq. 5 gives the relation between G and the mean surface velocity, V, over the impingement wall total surface area cooled by impingement cooling, A_s, which for a square array of holes is X^2.

Mean surface velocity V = m' / (ρA_s) = m' RT /PA_s
Thus   V/RT   = m'/ PA kg/(sm²Pa)
        V 10^5/(RT) = m'/PA kg/(sm²Bar) = G   (5)

Eq. 5 gives for a G of 2 kg/sm²bar a mean surface velocity at 700K coolant temperature of 4.0 m/s. The use of the coolant mass flow in terms of G enables the results at atmospheric pressure to be applied at engine pressures for the same coolant velocities. With impingement cooling the air velocity in the holes is defined by G and the hole area and is constant irrespective of the pressure.

EXPERIMENTAL METHODOLOGY

The experimental equipment [7, 14, 25, 26] is shown in Figure 2 and consists of an air supply to a thermally insulated plenum chamber feed to the impingement holes. The 152mm square Nimonic-75 impingement jet wall was bolted to the
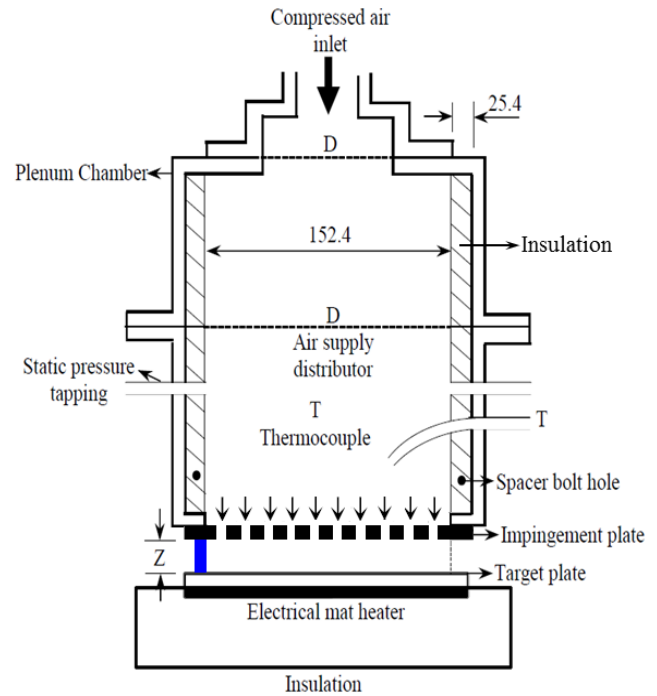

Figure 2 Single exit jet flow experimental test rig

plenum chamber exit flange. Nimonic-75 is a common combustor metal material, which was the reason for its choice as the test walls. An impingement gap Z of 10 mm was set using a PTFE spacer flange, which formed a one sided exit channel. The PTFE spacer has a low thermal conductivity and this minimized the transfer of heat between the two metal walls. The target wall was also Nimonic-75 and was 6.35mm thick. The impingement gap, Z, was varied by varying the thickness of the PTFE spacer flange.

The impingement jet wall and the target surface were instrumented with grounded junction mineral insulated Type K thermocouples that were brazed into the walls with the thermocouple tip flush with the jet wall discharge surface and the target wall impingement duct surface. The thermocouples were spaced on the centreline between the impingement jet holes at 25mm intervals from the start of edge of the test section. These were furthest from the point of impingement jet impingement and hence measured the highest temperature. Conduction in the metal wall was high (low Biot number, <0.1) and the wall temperature was locally uniform around each thermocouple, which measured the mean wall temperature. The CHT/CFD predictions confirm that the wall temperature was uniform local to each impingement jet.

The metal wall was heated electrically to about 80°C and then the coolant was initiated and the fall in temperature of the wall recorded for all 6 imbedded thermocouples. The cooling is a first order process and the time constant is proportional to the surface averaged heat transfer coefficient, h, as shown in Eqs. 6 and 7. The temperature of each thermocouples was recorded and Eq. 6 was plotted with dT_w/dt determined over 5s intervals. The slope of the line was the time constant and this was reproducible in repeat tests to better than +/- 5%. All the terms in Eq. 7 are fixed by the Nimonic material properties and the area of the test wall so that h was the unknown.

4

$$T_w - T_c = \tau \, dT_w/dt \qquad (6)$$

$$\text{where } \tau = mC/hA_p \qquad (7)$$

Also, the pressure loss from the air plenum to the exit duct wall downstream of the last impingement hole was measured based on Eq. 4. This was a key experimental measurement that had to be predicted well if the aerodynamics of the flow inside the impingement holes and the gap were correct. The experimental method gives no spatial resolution of h over the surface, but it gives reliable locally surface averaged h. This experimental technique has been shown to agree with other methods of measuring h in the literature for the same impingement geometry (1, 7, 14, 25, 26).

CFD METHODOLOGY

The symmetrical section that was modelled at each Z/D is shown in Fig. 3. The computational grid geometry is shown in Fig. 4 using the ANSYS ICEM CFD meshing. This symmetrical [28, 29] approach was applied for the prediction of the GT cooling systems that have been experimentally investigated using the experimental test rig of Fig. 2. The number of cells in the impingement gap, Z, varies as Z changes with an increased number of cells for larger values of Z. The cell size 'ξ' in the impingement gap was varied because of the differences in the impingement gap Reynolds number, Re, as the duct flow hydraulic diameter changes with Z.
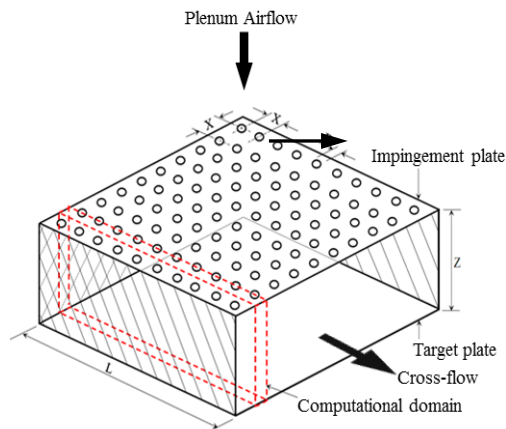
Figure 3 Computational domain and flow scheme

The standard k - ε turbulence model was found to be the only model that could predict correctly the flow separation and reattachment inside the wall thickness short holes [31], which was crucial to the correct prediction of the aerodynamics. The standard wall function near wall approach was also applied using the ANSYS Fluent CFD code. Grid independence tests were previously investigated [24,27] and the present number of cells in the hole and along the impingement gaps were found to be adequate. The first cell size near the target wall was maintained at a y^+ value of ~ 35 for all Z/D. This y^+ value is within the required near wall law of the wall range of $30 < y^+ < 300$. The choice of the y^+ values was based on the closer link [32] that they gave between the turbulent or log-log layer and the target wall, this was required for the good prediction of the wall heat transfer.
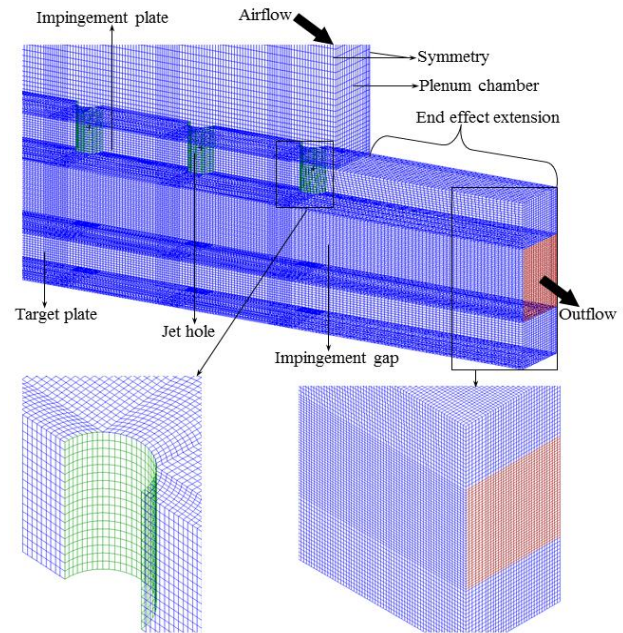

Figure 4 Impingement single exit jet flow grid geometry

PREDICTED FLOW-MALDISTRIBUTION

A feature of impingement cooling with single sided exit from the gap, as shown in Fig. 2, is that the pressure loss generated by the cross-flow can be significant in relation to the impingement wall pressure loss and this then generates a flow-maldistribution. Increasing Z/D at constant D decreases the cross-flow and this impact of crossflow was the major factor studied in the present work. El-jummah *et al* [28] have investigated the flow maldistribution effect of the crossflow for a fixed Z and variable D at constant X. This varied X/D from 1.9 – 11.0 with a Z/D variation of 1.2 – 7.3 . This did not change the crossflow mean velocity and hence varied the impingement wall pressure loss at fixed crossflow pressure loss. This showed that flow maldistribution in the crossflow direction was small for the present X/D of 4.7 and Z = 10mm (Z/D 3.1). If the impingement wall pressure loss was reduced by reducing X/D (larger D) then the flow maldistribution increased.

The crossflow effect was investigated in the present work at X/D = 4.7 by increasing the crossflow velocity by reducing Z or decreasing the crossflow velocity by increasing Z. This directly changed the crossflow velocity at constant impingement jet velocity. Another way of varying Z/D, keeping both X/D and Z constant is to vary the number of holes, n, at constant Z [33]. The authors have varied n from 1,076 – 26,910/m² at an X/D of 4.7 and the range of Z/D was 1.5 – 7.7. This did not cause a major change in the flow maldistribution as the crossflow and impingement jet relative pressure loss were not changed. At all Z/D the flow maldistribution from the mean flow per hole was -8% at the first hole to +8% at the last hole over the same 152mm axial distance. This previous work showed that the flow maldistribution was controlled by the absolute value of Z which controlled the mean crossflow velocity and that Z/D was not the controlling parameter.
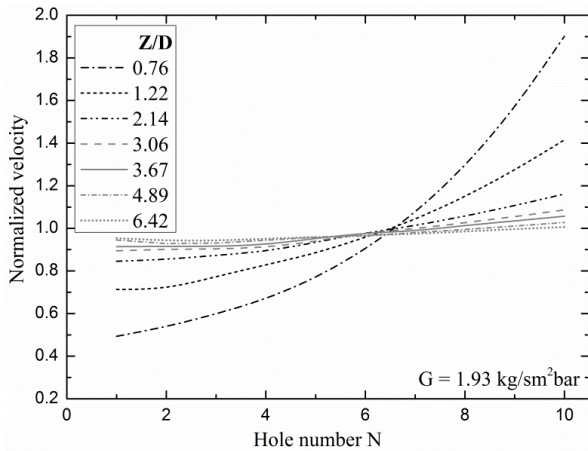
5

Figure 1 Impingement holes predicted flow-maldistribution

The present flow-maldistribution predictions for the range of Z in Table 1, were made based on the mass flow derived from the mean velocity in each hole at the midpoint of the hole length. Fig. 5 shows the ratio of the hole velocity to the mean velocity for all 10 rows of holes, $V_{j,}$ for the 10 holes in the impingement array. The 10mm gap, $Z/D = 3.06$, was a limiting condition with flow maldistribution at $<+/-10\%$ for Z/D of 3.06 or higher and very significant flow maldistribution for lower Z/D. For Z/D of 3.06 the total maldistribution of coolant mass flow between the last hole and the first was 16%, which is in good agreement with 1D flow predictions [27].

The action of the flow maldistribution will be shown to increase the downstream heat transfer and decrease the upstream heat transfer. However, the absence of flow maldistribution by using a large Z will be shown to result in reduced surface averaged heat transfer, as shown by Chance [8]. This was due to the reduction of the impingement velocity of the original jet fluid on the cooled wall as Z becomes larger.

PREDICTED IMPINGEMENT GAP AERODYNAMICS

The predicted streamlines for the flow after the hole outlet and in the gap are shown in Fig. 6 for the baseline Z of 10mm, Z/D = 3.06. For the second hole in the impingement hole array in Fig. 6a the aerodynamics are not significantly influenced by the crossflow as there is only one upstream row of holes. The flow patterns show the impingement jet hitting the target surface directly below the impingement jet and then interacting with adjacent impingement jets on the surface to produce a reverse flow on the centreline of the square array of holes, which is the corner region in Fig. 6a. The crossflow velocity increases, as more impingement holes feed air into the crossflow, and is at a maximum just upstream of the last hole. The aerodynamics at hole 9 are shown in Fig. 6b and this shows that the crossflow deflects the reverse flow jet, which is inline with the crossflow, as well as deflecting the impingement jet. At higher Z the crossflow velocity decreases and this decreases the deflection of the impingement jet, but the deflection of the reverse flow jet was still significant.
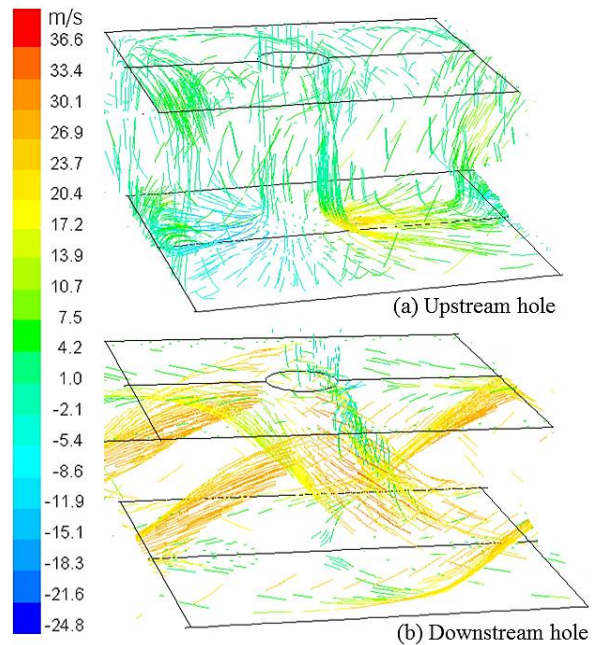

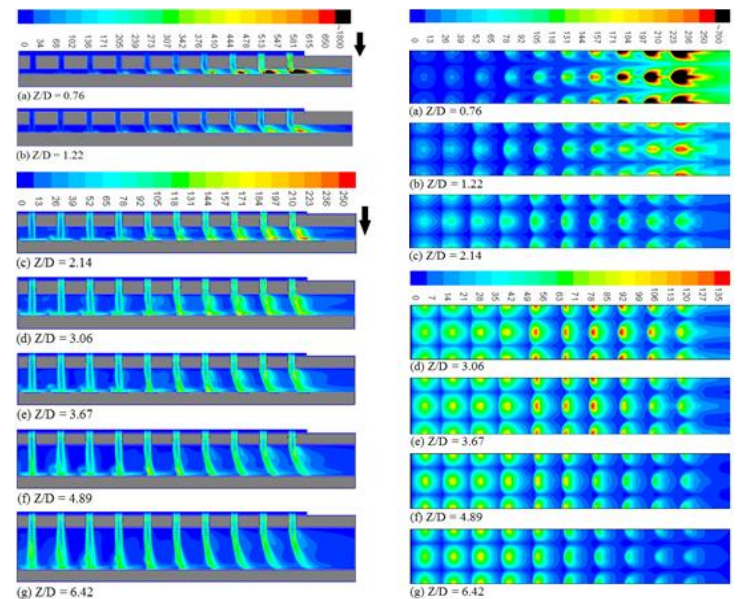**Figure 6** Impingement gap predicted velocity (m/s) streamlines for Z/D of 3.06, Z of 10mm

Figure 7 Predicted distribution of turbulent kinetic energy, m^2s^2 for varied Z and Z/D at G = 1.93 kg/sm^2bar: LHS impingement jet centreline plots; RHS surface distribution of kinetic energy.

The profiles of turbulent kinetic energy on the centreline of the impingement jets are shown in Fig. 7 (LHS) as a function of Z/D. This shows the concentration of turbulence in the shear layer at the edge of the jets for large Z/D. At low Z/D the flow maldistribution results in most of the turbulence being associated with the downstream jets that have a higher jet mass flow and jet velocities. At large Z/D the deflection of the impingement jets by the crossflow is clearly seen in the turbulent kinetic energy distribution, which is convected downstream by the crossflow.
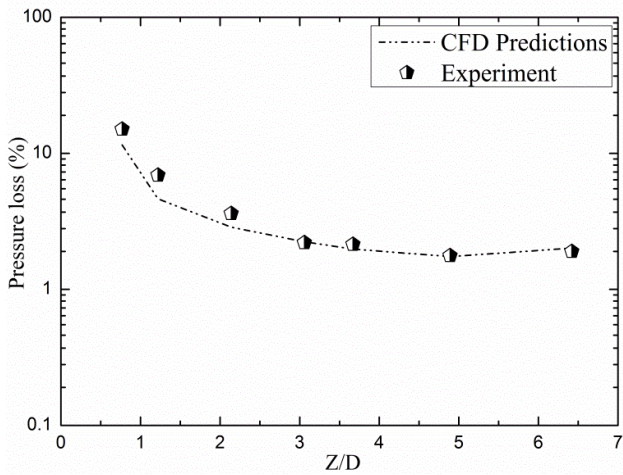
6

Figure 8 Comparison of the predicted and measured pressure loss as a function of Z/D for G = 1.93 kg/sm²bar
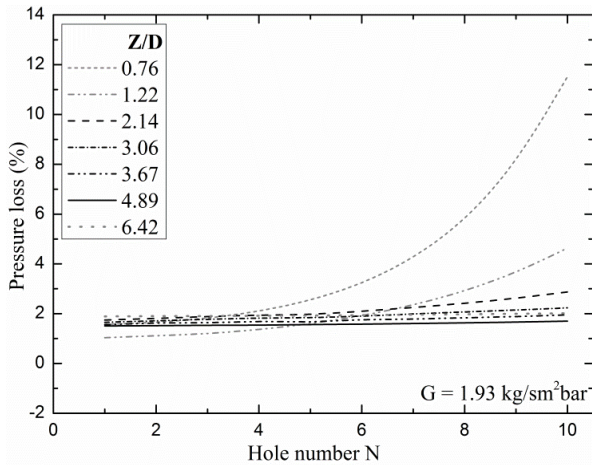

Figure 9 Predicted pressure loss as a function of the hole number along the impingement gap.

The surface heat transfer is controlled by the surface distribution of turbulence and the predictions of this for all the Z/D modelled are shown in Fig. 7. This also shows the strong influence of the flow maldistribution at low Z/D, with most of the high turbulence regions in line with the downstream jets, which have the higher mass flow. At Z/D of 3.7 or higher the peak turbulence is inline with the impingement jets at the upstream part of the test wall. Much lower surface turbulence was predicted in the downstream portion of the test wall, where the jet turbulence is deflected and turbulence only occurred in the downstream protion of the jet. Thus there is less surface covered with high turbulence and this results in lower heat transfer.
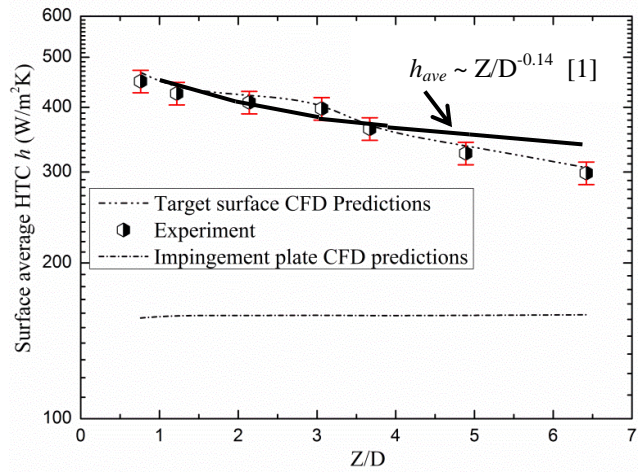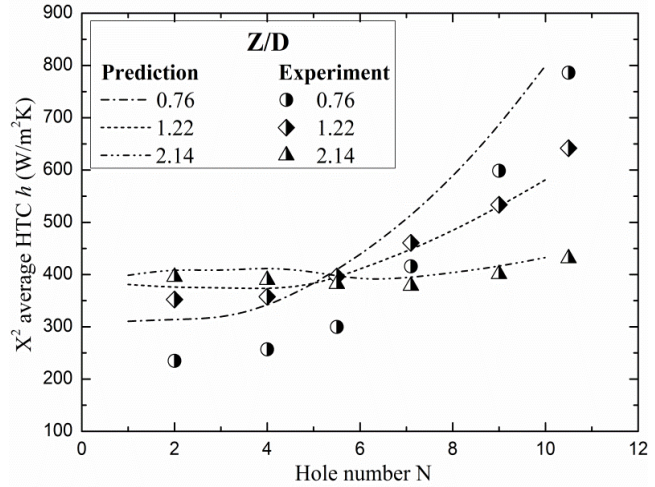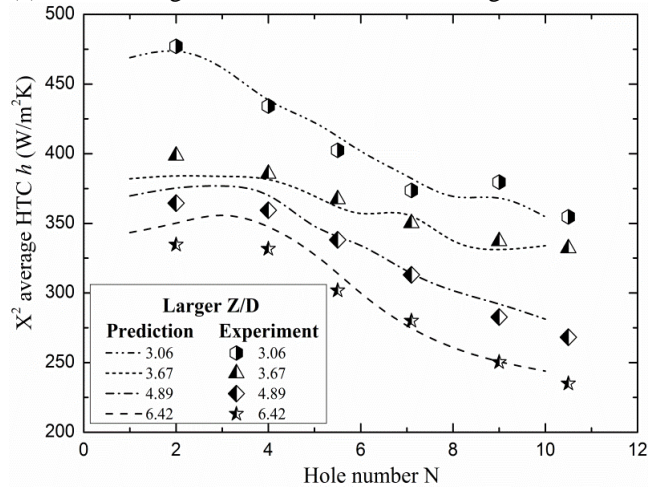

Figure 10 Comparison of Z/D predicted and experimental surface average HTC h for target and impingement walls

(a) Smaller range of Z/D at fixed G of 1.93 kg/sm²

(b) Larger range of Z/D at fixed G of 1.93 kg/sm²

Figure 11 Comparison of Z/D predicted and experimental X^2 average HTC h on the target wall at constant X/D and G

7

COMPARISON OF THE MEASURED AND PREDICTED PRESSURE LOSS

The overall impingement wall pressure loss was measured and predicted as the static pressure difference between the air supply plenum chamber in Fig. 2 and the impingement jet wall well downstream of the last hole, but before the exit plane. The location of the static pressure at the discharge plane was on the centreline between the impingement jet holes, where the static pressure recovery in the expansion of the last impingement jet had occurred. The predicted and measured pressure loss are compared in Fig.8. The agreement is very good for Z/D =>3, but there was a slight under prediction for lower Z/D where the crossflow velocity was highest. The good agreement in predicted pressure loss shows that the predicted aerodynamics must be adequately predicted as these dominate the pressure loss.

The axial variation of the pressure loss was predicted using the plenum chamber static pressure as reference and the static pressure predicted at the centreline between the jets on the impingement jet wall. These predicted results are shown in Fig. 9 as pressure loss as a function of the hole number. This shows that where there is a significant flow maldistribution predicted for Z/D<3, there is an axial variation of pressure loss, which was very large at the lowest Z/D. At Z/D > 3 there was little or no axial variation of the pressure loss along the crossflow gap.

At large Z/D the pressure loss at G=1.93 kg/sm^{2}bar was 2.0% and this is about the maximum that could be allocated to the regenerative backside combustor wall cooling in a low NOx combustor. A lower pressure loss would be preferable and this would require a lower X/D.

HEAT TRANSFER COEFFICIENT, *h*

The surface averaged heat transfer coefficient, h_{ave}, measurement and predictions are compared in Fig. 10. The measured h_{ave} was the mean of the six local surface average heat transfer thermocouple responses. The agreement of the measurements with the predictions was excellent and within the +/-5% error band of the measurements. This indicates that the CHT/CFD computational procedures for the surface averaged heat transfer were good. Fig. 10 shows that h_{ave} decreased as Z/D increased, but in the range of Z/D 1-3 there was only a small decrease of 5%.

This relatively low influence of Z/D was also shown experimentally by Andrews and Hussain [1] for four sided exit flow, where for an X/D of 2.9 the Z/D dependence was an exponent of -0.14. In the present work this Z/D dependence would give a reduction in h_{ave} from 450 W/m^{2}K at Z/D of 1 as shown by the trend line [1] in Fig. 10 and are in good agreement with the experimental results up to a Z/D of 4 and then the predictions are a little high.

The axial variation of the locally X^2 surface averaged heat transfer is compared with the predictions in Fig. 11. The agreement was good at all Z/D apart from the smallest Z/D of 0.76, where the predictions were lower than the measurement, but the effect of flow maldistribution on the local heat transfer was well predicted. The trend for Z/D of 3.06 or higher is that
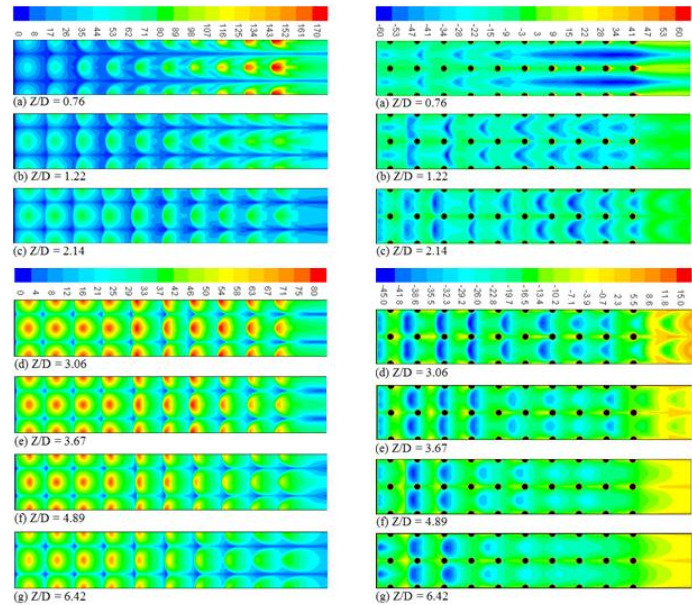

Figure 12 Predicted surface distribution of the Nu for the target wall (left) and impingement jet wall (right) for Z/D 0.76-6.4 for a G=1.93 kg/sm^{2}bar.

the locally surfaced averaged heat transfer coefficient decreased with axial distance, due to the adverse influence of crossflow. At lower Z/D the flow maldistribution that resulted from the higher crossflow resulted in higher heat transfer in the downstream part of the crossflow.

The predicted surface distribution of the Nu is shown in Fig. 12 (left) for the impingement jet target surface and in Fig. 12 (right) for the impingement jet hole surface. The predicted Nu distribution on the target surface is very similar to the predicted surface distribution of turbulent kinetic energy in Fig. 10 (right). This shows that the heat transfer on the target surface is controlled by the generation of turbulence by the impingement jets. Fig. 12 also shows the same trends as for the locally surface average heat transfer in Fig. 11. At low Z/D the flow maldistribution leads to higher coolant air mass flow in the downstream jets with associated higher peak heat transfer. For Z/D>2 the reverse trend occurs with higher heat transfer by the initial holes and lower heat transfer downstream. For a Z/D of 6.4 the downstream impingement jets do not reach the target surface and the peak heat transfer is very low compared with lower Z/D.

The heat transfer due to the reverse flow jets on the impingement jet hole surface in Fig. 12 is –ve as it is heat transfer in the opposite direction to that on the target surface, this surface is being heated by the reverse jet flow rather than cooled. The peak Nu is about a third of the peak Nu on the target surface. The predicted high Nu at the impact of the reverse flow jet on the centre point of each group of four impingement holes is shown in Fig. 12 at all Z/D. The impact of the crossflow is predicted to be a strong deflection of the reverse flow jet by the crossflow, so that the point of high Nu on the jet wall moves downstream. Fig. 12 shows for a Z/D of 3.06 and higher only 7 reverse jet flow impact points for the 10 rows of holes, due to the action of the crossflow. The deflection of the reverse flow jet by the crossflow is shown in Fig. 6.
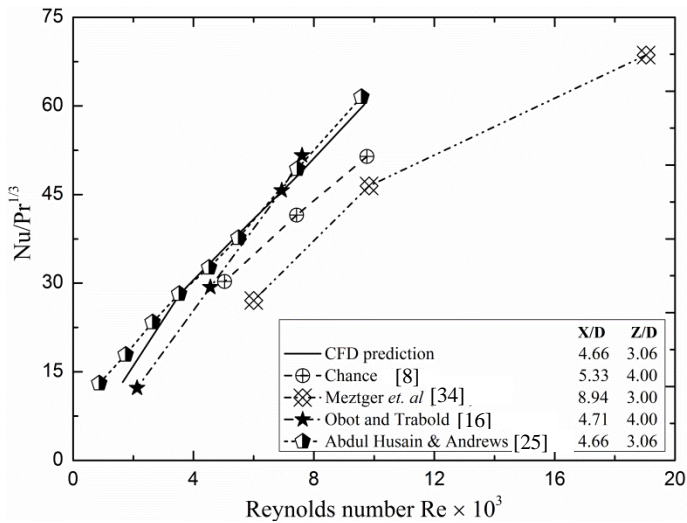
8

Figure 13 Comparison of the present predictions with literature experimental measurements for similar geometries.

The present predictions are compared in Fig. 13 with literature measurements for similar Z/D for surface averaged predictions and measurements. In addition to the good agreement with the results of Abdul Husain and Andrews [25] there is very good agreement with the results of Obot and Trebold [16]. The other results are below the predictions due to differences in X/D.

DIMENSIONLESS TEMPERATURE PREDICTIONS

The distribution of dimensionless gas temperatures, T*, as defined in Eq. 7, are shown in Fig. 14.

$$T^* = \frac{(T - T_\infty)}{(T_w - T_\infty)} \tag{7}$$

Fig.14 also shows the distribution of the temperature in the wall and for this the wall temperature in Eq. 7 is replaced by the heated wall surface temperature, T_s. Fig. 14 shows in the planes between the impingement jets, a clear depiction of the heated reverse flow jets and the deflection of these jets by the crossflow.

Fig. 14 shows that for Z/D >3.06 the reverse flow jets do not reach the impingement jet wall and in the worst case at Z/D = 6.42 the heated coolant remains in the vicinity of the cooled wall, giving a poor convective heat transfer, as shown in Figs. 11b and 12. At high Z/D Fig. 14 shows that the heating of the coolant is confined to the reflected jet. However, as Z/D is reduced this heating is transferred to the higher velocity crossflow and the whole crossflow takes part in the removal of heat. This is why the heat transfer is so high at low Z/D and when the flow maldistribution is added this gives extremely

high convective heat transfer in the downstream portion of the target wall, as shown in Fig. 11a.
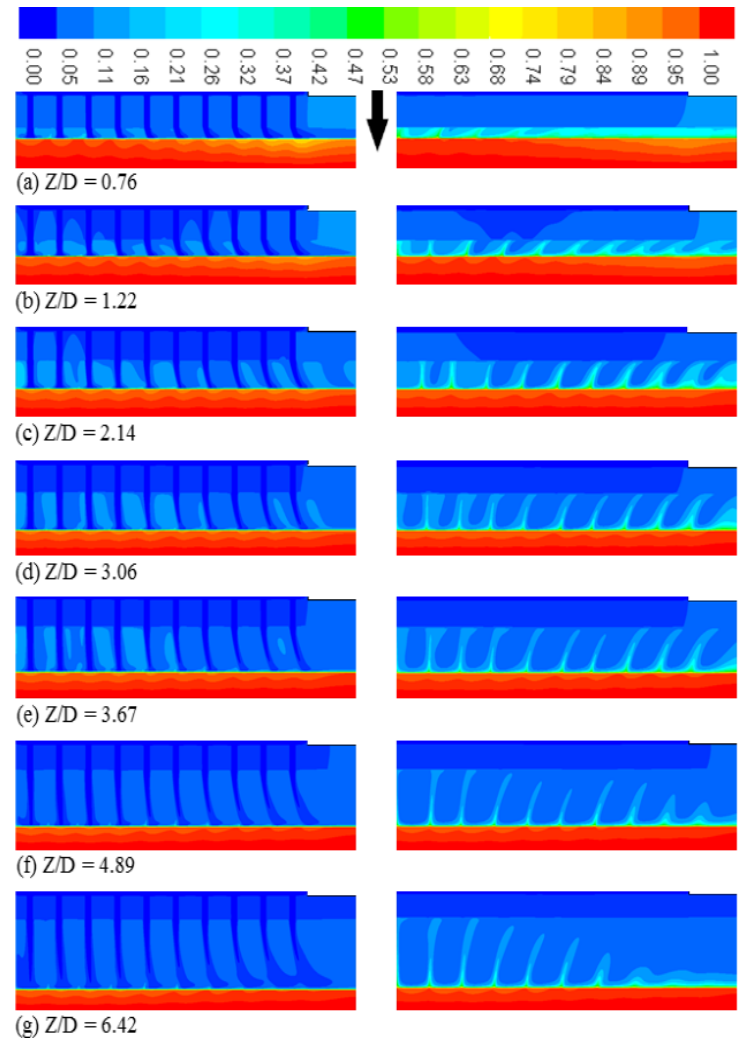

Figure 14 Predicted variation of T^* for a range of Z/D: centre line of the impingement jets (left) and between the impingement jets (right).

SURFACE DISTRIBUTION OF TEMPERATURE

The predicted dimensionless surface distribution of the target wall temperature is shown in Fig. 15 for a range of Z/D at G = 1.93 kg/sm²bar. These predictions include the conjugate heat transfer by conduction inside the metal wall. The result of the internal conduction is for there to be much lower metal temperature gradients than gradients in heat transfer coefficient and Nu in Fig. 12 (left). For example for a Z/D of 3.06 in the leading edge region, the axial surface gradient in Nu is at least +/- 30% of the mean Nu and the gradients in T* at the same location is only +/- 3% of the mean. This is a reduction of a factor of 10 in the metal temperature gradients compared with the convective heat transfer surface gradients.
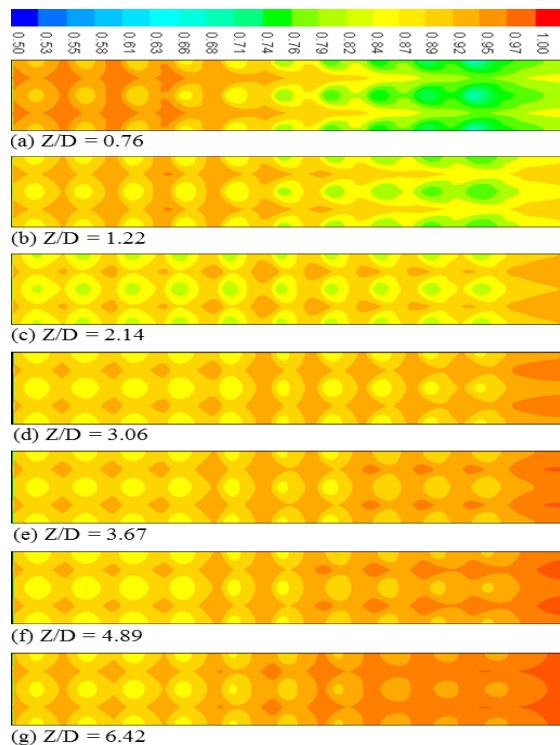
9

(a) Z/D = 0.76

(b) Z/D = 1.22

(c) Z/D = 2.14

(d) Z/D = 3.06

(e) Z/D = 3.67

(f) Z/D = 4.89

(g) Z/D = 6.42

Figure 15 Predicted surface distribution of dimensionless metal temperature, T^*, for a range of X/D.

Figure 16 Predicted locally surfaced avaerage T^* as a function of the impingement hole number for a range of Z/D at G = 1.93 kg/sm^2bar.

Fig. 15 shows that in addition to the metal temperature gradients in the vicinity of each impingement point, there is a temperature change of similar magnitude along the length of the impingement gap. This corresponds to the change with distance of the locally surface averaged heat transfer coefficient in Fig. 11. The X^2 surface averaged T^* are shown as a function of the hole number in Fig. 16. This shows that the significant axial gradients in locally surface averaged heat transfer coefficients result in smaller surface averaged temperature gradients in the metal target wall.

Fig. 16 shows a quite different axial profile for the smallest impingement gap, where the flow maldistribution was very significant as shown in Fig. 5. The locally surface averaged T^* gradients with hole number are similar to those for the locally surface averaged h in Fig. 11. For the Z/D of 3.06 the deviation from the whole surfaced averaged condition is +/- 15% for both T^* and h. Thus these relatively long distance surface temperature difference are controlled by the axial gradients in surface averaged heat transfer coefficients and not by internal wall conduction. However, local to each impingement point the large local gradients in h and Nu are greatly reduced by internal wall conduction.

CONCLUSIONS

Experimental and numerical investigations were carried out on impingement jet cooling, for variable gap to diameter ratio Z/D ranging from 0.76 - 6.42 with varied Z, constant D and constant mass flux G of 1.93 kg/sm^2bar, which is typical of G
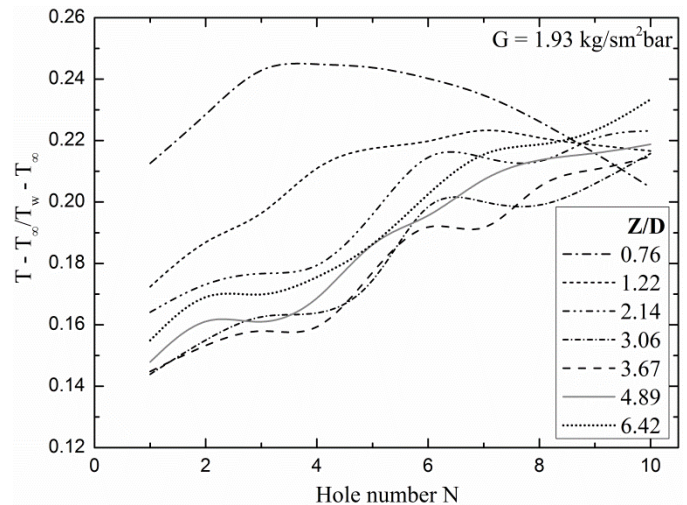
for regenerative backside cooling of gas turbine combustors. This is the cooling geometry relevant to reverse flow cylindrical combustors with low NOx burners, where air used for film cooling increases the NOx. The geometries investigated were for 10×10 square arrays of impingement jet cooling holes at constant diameter D and pitch X, hence constant X/D ratio.

Conjugate heat transfer (CHT) computational fluid dynamics (CFD) were applied to the same geometries. The predicted CFD results agreed with the measured pressure loss, which indicates that the predicted aerodynamics were good. Also, the locally X^2 and overall surface average heat transfer coefficients (HTC) h were well predicted, apart from at the lowest Z/D.

High flow maldistribution between the 10 rows of impingement jets was predicted to occur for Z/D below 3.06, where the flow maldistribution was >+/-10%. The action of the flow maldistribution was shown to increase the downstream heat transfer and decrease the upstream heat transfer, as found experimentally. However, the absence of flow maldistribution by using a large Z was shown to result in reduced surface averaged heat transfer. This was due to the reduction of the impingement velocity of the original jet fluid on the cooled wall as Z becomes larger.

In the planes between the impingement jets, there is a reverse flow jets that is heated by the target wall heat transfer. This reverse flow jet is strongly deflected by the crossflow. For Z/D >3.06 the reverse flow jets do not reach the impingement jet wall and in the worst case at Z/D = 6.42 the heated coolant remains in the vicinity of the cooled wall, giving a poor convective heat transfer. At high Z/D the heating of the coolant was confined to the reflected jet.

10

However, as Z/D was reduced this heating was transferred to the higher velocity crossflow and the whole crossflow takes part in the removal of heat. This is why the heat transfer is so high at low Z/D and when the flow maldistribution is added this gives extremely high convective heat transfer in the downstream portion of the target wall.

ACKNOWLEDGEMENTS

REFERENCES
[1] Andrews G. E. & Hussain C. I. 1984. Impingement Cooling of Gas Turbine Components. *High Temperature Technology,* 2 (2)**,** 99 - 106.

[2] Andrews, G.E. and Kim, M.N. The influence of film cooling on emissions for a low radial swirler gas turbine combustor, ASME Paper 2001-GT-71, presented at the ASME International Gas Turbine & Aeroengine Congress & Exhibition, New Orleans (2001).

[3] Reiss F., Wiers S-H., Orth U., Aschenbruck E., Lauer M. & El Masalme J. 2014. Combustion System Development and Testing for MAN's New Industrial Gas Turbines MGT 6100 and MGT 6200. *Proc. ASME Turbo Expo,* GT2014-25907**,** 1 - 9.

[4] Facchini B. and Surace M., "Impingement Cooling for Modern Combustors: Experimental Analysis of Heat Transfer and Effectiveness," *Experiments in Fluids. Springer,* vol.40, pp.601-611, 2006.

[5] Andrews G. E. and Hussain C. I., "Full Coverage Impingement Heat Transfer: The Influence of Crossflow," *AIAA-87-2010,* pp. 1-9, 1987.

[6] Kercher D. M. and Tabakoff W., "Heat Transfer by a Square Array of Round Air Jets Impinging Perpendicular to a Flat Surface including Effects of Spent Air," *ASME J. Eng. Power,* pp. 73-82, 1970.

[7] Abdul Husain R. A. A., Andrews G. E., Asere A. A., and Ndiema C. K. W., "Full Coverage Impingement Heat Transfer: Cooling Effectiveness," *ASME Int. Gas Turbine Conference,* 88-GT-270, pp. 1 - 9, 1988.

[8] Chance J. L., "Experimental Investigation of Air Impingement Heat Transfer under an Array of Round Jets," *Tappi,* vol.57, No.6, pp. 108-112, 1974.

[9] Florschuetz L. W., Truman C. R., and Metzger D. E., "Streamwise Flow and Heat Transfer Distributions for Jet Array Impingement with Crossflow," *Trans. ASME, J. Heat Transfer,* vol.103, pp. 337-342, 1981.

[10] Freidman S. J. and Mueller A. C., "Heat Transfer to Flat Surfaces," presented at the ASME Proc. General Discussion on Heat Transfer. Inst. Mech. Engineers, pp.138-142, 1951.

[11] Huang G. C., "Investigations of Heat Transfer Coefficients for Air Flow Through Round Jets Impinging Normal to a Heat Transfer Surface," *ASME J. Heat Transfer,* pp.237-245, 1963.

[12] Hollworth B. R. and Berry R. D., "Heat Transfer from Arrays of Impinging Jets with Large Jet-to-Jet Spacing," *ASME Paper No. 78-GT-117,* pp. 1-6, 1978.

[13] Saad N. R., Mujumdar A. S., Abdel Messah W., and Douglas W. J. M., "Local Heat Transfer Characteristics for Staggered Arrays of Circular Impinging Jets with Crossflow of Spent Air," *ASME paper No. 80-HT-23,* pp. 1-8, 1980.

[14] Andrews G. E., Asere A. A., Hussain C. I., and Mkpadi M. C., "Full Coverage Impingement Heat Transfer: The Variation in Pitch to Diameter Ratio at a Constant Gap," *Proportion and Energetics Panel of AGARD, 65th Symposium, 'Heat Transfer and Cooling in Gas Turbines',* vol. 26, pp. 1-12, 1985.

[15] Metzger D. E. and Korstad R. J., "Effects of Crossflow on Impingement Heat Transfer," *ASME J. Eng. Power,* pp. 35-41, 1972.

[16] Obot N. T. and Trabold T. A., "Impingement Heat Transfer within Arrays of Circular Jets: Part 1-Efects of Minimum, Intermediate and Complete Crossflow for Small and Large Spacings," *J. Heat Transfer. Transactions of the ASME,* vol.109, pp.872-879, 1987.

[17] Andrews G. E. and Hussain C. I., "Full Coverage Impingement Heat Transfer: Influence of Channel Height," presented at the Eight International Heat Transfer Conference, 1986.

[18] Andrews, G.E., Alkabie, H.S., Abdul Hussain, U.S. and Abdul Aziz, M. Ultra low NOx ultra lean gas turbine primary zones with liquid fuels. AGARD 81st Symposium of the Propulsion and Energetics Panel of Fuels and Combustion Technology for Advanced Aircraft Engines. AGARD Conference Proceedings pp.24.1-24.14 (1993).

[19] Bailey J. C., Intile J., Fric T. F., Tolpadi A. K., Nirmalan N. V., and Bunker R. S., "Experimental and Numerical Study of Heat Transfer in a Gas Turbine Combustor Liner," *J. Eng. Gas Turbines and Power. Transactions of the ASME,* vol.125, pp.994-1002, 2003.

[20] Taslim M. E. and Rosso N., "Experimental/Numerical Study of Multiple Rows of Confined Jet Impingement Normal to a Surface at Close Distances," *Proceedings of ASME Turbo Expo 2012*, Copenhagen, 2012, pp. 1-13.

[21] Rao G. A., Levy Y., and Belinkov M. K., "Numerical Analysis of a Multiple Jet Impingement System," in *proc. ASME Turbo Expo 2009*, Florida, 2009, pp. 1-11.

[22] Anand K. and Jubran B. A., "Computational Study of Micro-jet Impingement Heat Transfer in a High Pressure Turbine Vane," *Proc. ASME Turbo Expo* 2011, pp. 1-12.

[23] Andrews G. E., Wang J., and Abdul Husain R. A. A., "CFD Predictions of the Aerodynamics and Heat Transfer from Arrays of Impingement Jets with crossflow," *IGTC*, Osaka, 2011, pp.1-18.

[24] El-jummah A. M., Andrews G. E., and Staggs J. E. J., "Conjugate Heat Transfer CFD Predictions of Impingement Jet Array Flat Wall Cooling Aerodynamics with Single Sided Flow Exit," *Proceedings of ASME Turbo Expo 2013*, GT2013-95343.

[25] Abdul Husain R. A. A. & Andrews G. E. 1990. Full Coverage Impingement Heat Transfer at High Temperature. *Proc. ASME Int. Gas Turbine & Aeroengine Congress & Eposition,* 90-GT-285**,** 1 - 12.

11

[26] Andrews, G.E., Durance, J., Hussain, C.I. and Ojobar, S.N. Full coverage impingement heat transfer: the influence of the number of holes, Transactions of the ASME, Journal of Turbomachinery, Vol.104, pp.557-563 (1987).

[27] El-jummah, A. M., Andrews, G. E. & Staggs, J. E. J. 2013. Conjugate Heat Transfer CFD Predictions of the Influence of the Impingement Gap on the Effect of Cross-Flow. *Proc. ASME Heat Transfer Conference,* HT2013-17180**,** 1 - 12.

[28] El-jummah A. M., Abdul Hussain R. A. A., Andrews G. E. & Staggs J. E. J. 2014. Conjugate Heat Transfer Computational Fluid Dynamic Predictions of Impingement Heat Transfer: The Influence of Hole Pitch to Diameter Ratio X/D at Constant Impingement Gap Z. *Trans. ASME J. Turbomachinery,* 136 (12)**,** 1 - 16.

[29] El-jummah A. M., Andrews G. E. & Staggs J. E. J. 2016. Impingement/Effusion Cooling Wall Heat Transfer: Conjugate Heat Transfer Computational Fluid Dynamic Predictions. *Proc. ASME Turbo Expo: Turbomachinery Technical Conference & Exposition,* GT2016- 56961**,** 1 - 12.

[30] El-jummah A. M., Andrews G. E. & Staggs J. E. J. 2015. CHT/CFD Predictions of Impingement Cooling With Four Sided Flow Exit. *Proc. ASME Turbo Expo,* GT2015-42256 1 - 12.

[31] El-jummah A. M., Andrews G. E. & Staggs J. E. J. 2015. Conjugate Heat Transfer CFD Predictions of Metal Walls with Arrays of Short Holes as Used in Impingement and Effusion Cooling. *Proc. GTSJ Int. Gas Turbine Congress,* IGTC TS - 266**,** 1 - 9.

[32] Nuutinen M., Kaario O. & Larmi M. 2009. Advances in Variable Density Wall Functions for Turbulent Flow CFD-Simulations, Emphasis on Heat Transfer. *SAE International,* 2009-01-1975**,** 1 - 16.

[33] El-jummah A. M., Abdul Hussain R. A. A., Andrews G. E. & Staggs J. E. J. 2014. Conjugate Heat Transfer CFD Predictions of Impingement Heat Transfer: The Influence of the Number of Holes for a Constant Pitch-to-diameter Ratio, X/D. Proc. ASME Turbo Expo, Dusseldorf. ASME Paper GT2014-25268.

[34] Metzger D. E., Florschuetz L. W., Takeuchi D. I., Behee R. D. and Berry R. A. 1979. "Heat Transfer Characteristics for Inline and Staggered Arrays of Circular Jets With Cross-Flow of Spent Air". *Trans. ASME J. Heat Transfer,* 101**,** 526 - 531.

12